JOURNAL OF MATERIALS SCIENCE 23 (1988) 2772–2785

Analysis of the friction (spin)-welding process for thermoplastics

VIJAY K. STOKES
General Electric Company, Corporate Research and Development, Schenectady, New York 12301, USA

The friction (spin)-welding process for thermoplastics is known to consist of four phases: (1) initial heating of the interface to the melting temperature by Coulomb friction, (2) unsteady melting and flow in the transverse direction, (3) steady-state flow, and (4) unsteady flow and solidification after the spin motion is stopped. Simple analytical models, which are based on an analysis of the vibration welding process, have been developed for the first three phases. These models have been used for analysing spin-welding data for poly(methyl methacrylate), poly(vinyl chloride), acetal and nylon 66. Estimates have been obtained for the film thickness, the film viscosity and the film temperature as functions of the weld process parameters. In particular, it has been shown that an increase in the weld velocity can result in a significant reduction of the film viscosity. The film viscosity is shown to be less sensitive to the weld pressure.

1. Introduction

The purpose of this paper is to analyse the friction (spin)-welding process for thermoplastics. Spin welding can be used for bonding thermoplastic components along plane mating surfaces. In this process, the parts to be joined are rotationally rubbed relative to each other, under pressure, about an axis normal to the plane surfaces to be joined, as schematically shown in Fig. 1. The resulting frictional heating at the plane interface causes the plastic to heat up and melt. When the relative motion is stopped, the molten film solidifies under pressure, resulting in a weld.

The main process parameters for spin welding are the weld velocity (relative rubbing speed), w_0, the weld pressure, p_0, and the weld time. Once the interface begins to melt, the weld pressure, p_0, will cause the molten material to flow laterally outwards, thereby continuously decreasing the distance between the parts being welded. This decrease in distance, η, may be called weld penetration. The interfacial welding torque, T, is the torque required for producing the relative rotary rubbing motion at the weld interface. In order to study systematically the effects of these process parameters on the weldability of thermoplastics, Crawford and Tam [1] built an instrumented spin-welding machine in which each of the four parameters, w_0, p_0, η, and T, can be monitored continuously. They used this machine to investigate the weld phenomenology for the two amorphous thermoplastics, poly(methyl methacrylate) (PMMA) and poly(vinyl chloride) (PVC), and the two semicrystalline thermoplastics, acetal and nylon 66. Their data are in the form of plots of the steady-state welding torque and the penetration rate (which they call the burn-off) against the weld velocity, with the weld pressure as parameter; and plots of the steady-state welding torque and the penetration rate against the weld pressure, with the weld velocity as parameter.

While Crawford and Tam [1] understood that a molten viscous film is formed at the interface during the welding process, they attempted to derive equivalent coefficients of solid friction which, according to them, ". . . are, therefore, probably more akin to a coefficient of shear viscosity". They also realized that a more complete analysis would be required for explaining the trends exhibited by their data: "However, it is apparent that some complex interaction of material properties must influence the amount of burn-off because PVC, which heats up more slowly than the other materials and is generally regarded as having a high melt viscosity, does in fact exhibit a much greater burn-off rate than any of the other materials".

The friction (spin)-welding process is very similar to the vibration (linear)-welding process for thermoplastics. Both processes rely on frictional heating for melting the interface. The main difference is that in vibration welding the frictional heating is achieved via a vibratory shear motion. Both these processes have many potential advantages: (1) relatively short cycle times, (2) simple equipment, and (3) insensitivity of the processes to weld surface preparation. In contrast to adhesive bonding, no foreign material is introduced, so that the weld interface is of the same material as the parts to be welded. Also, in contrast to hot plate welding, in which the interfaces to be welded are heated conductively by direct contact with a hot plate, the heating is very localized. Moreover, the vibration- and spin-welding processes are far more controllable and are much less likely to cause material degradation because of overheating at the interface.

This paper is aimed at developing an anaysis for the spin-welding process, and at using this analysis for

0022–2461/88 $03.00 + .12

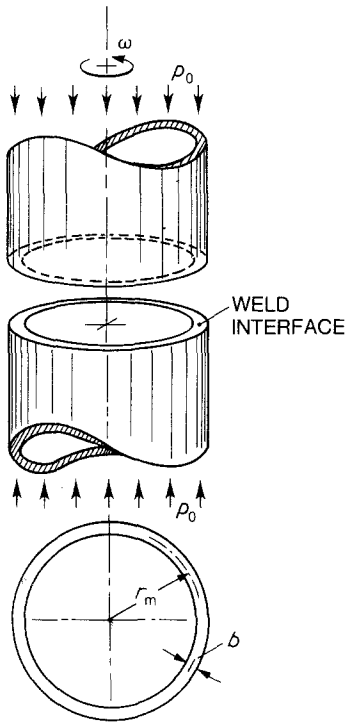

Figure 1 Schematic representation of the friction (spin)-welding process.

evaluating Crawford and Tam's data. The analysis parallels the analysis of the vibration (linear)-welding process developed previously [2–4].

2. Weld phenomenology

The typical qualitative variations of the weld parameters, w_0, p_0, T, and η, with time are shown in Fig. 3 in [1], in which the axes have not been scaled. The penetration (burn-off) transducer first shows a linear increase with time, during which the surfaces are being brought towards each other, but do not touch. When contact is made, the torque T, and weld pressure, p, increase with time – apparently linearly with time – until the pressure reaches the steady-state value, p_0. The torque also appears to attain a steady state. Once contact is made, the penetration increases slightly and then remains constant for some time. During this phase of constant (zero) penetration, the surface is being heated by Coulomb friction, culminating in a

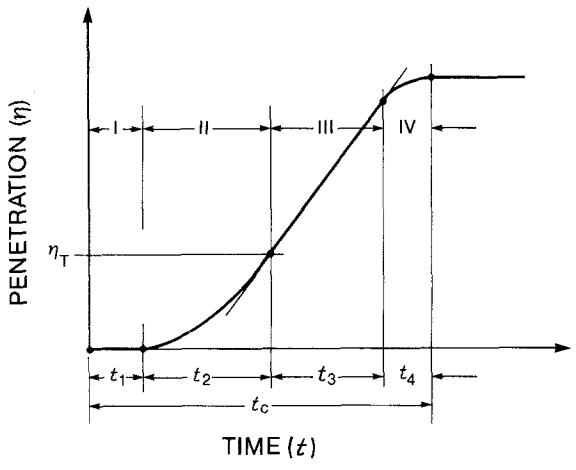

Figure 2 Schematic penetration–time curve showing four regimes of the friction (spin)-welding process.

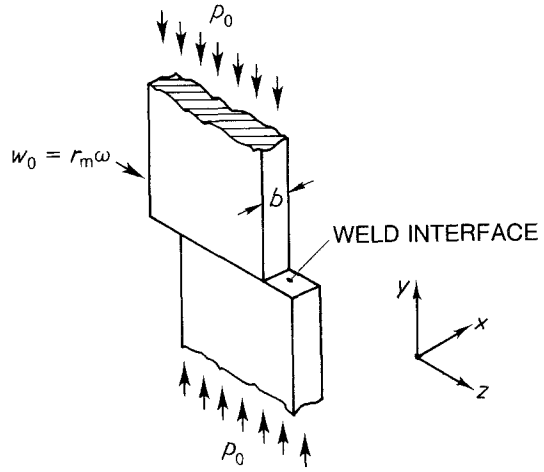

Figure 3 One-dimensional model for the friction (spin)-welding process. w_0 = weld velocity, p_0 = weld pressure.

melting of the interfacial material. The molten film begins to flow laterally outwards, resulting in an increase of penetration with time. Soon a steady state is reached, in which the rate of melting equals the rate of outflow, during which the penetration increases linearly with time. Once the weld motion is stopped, the molten film continues to flow while cooling. This results in a further continuing increase in penetration.

Fig. 3 in [1] only has one set of curves showing the simultaneous variations of the weld parameters with time, and the axes representing the parameters and time are not scaled. Furthermore, most of the data are for the steady-state phase, while the Coulomb-friction and unsteady-state phases have been compressed into a small part of the curves. As mentioned earlier, the spin-welding process is very similar to the vibration-welding process, on which more information is available [2–4]. There is every reason to believe that the penetration–time behavior of thermoplastics would be the same in spin and in vibration welding.

A detailed investigation of the vibration welding of four thermoplastics has shown [2] that the welding process can broadly be divided into four distinct phases, which are shown on the schematic penetration–time curve in Fig. 2. In Regime I, of duration, t_1, there is no penetration, η, and the interface heats up to the "melting" temperature by Coulomb frictional heating. This is followed by Regime II, in which the interface begins to melt, resulting in unsteady flow in the lateral direction. A steady state is attained in Regime III, in which the rate of melting at the solid–liquid interface equals the rate at which the molten material is being extruded out laterally. In Regime IV the weld motion is stopped, but the weld pressure causes the lateral outflow from the film to continue. At the same time the film cools and solidifies forming the desired weld at the interface. The total weld time, or "cycle time", is the sum $t_c = t_1 + t_2 + t_3 + t_4$ of the times for each of these four regimes.

On the basis of the curves in Fig. 3 of [1] and the descriptions of these curves [1], it will be assumed that Fig. 2 also describes the phenomenology of the spin-welding process. However, Crawford and Tam [1] only give data for the steady-state phase of spin welding (Regime III). What is available are curves of the

penetration rate, $\dot{\eta}$, and the steady-state weld torque, T_0, against the weld velocity, w_0, and against the weld pressure, p_0. As such, the bulk of the analysis effort will be devoted to this steady-state phase.

Fig. 1 shows the geometry for the spin welding of tubes. As the mean radius, r_m, of the tubes will normally be much larger than the tube thickness, b, the problem is equivalent to the one-dimensional problem shown in Fig. 3. The cylindrical geometry is replaced by two semi-infinite plates of thickness, b, that slide relative to each other, along their common interface, with a constant sliding velocity $w_0 = r_m\omega$.

3. Heat generation by solid friction (Regime I)

In the model problem for the temperature rise at the weld interface caused by frictional heating, the weld interface is the x–z plane, with the relative motion occurring in the z-direction, as is shown in Fig. 4. The y-direction is normal to the weld surface.

The instantaneous rate of heat generation per unit interfacial area, q_0, is given by

$$q_0 = fp_0w_0 \tag{1}$$

where w_0 is the interfacial relative velocity, p_0 the interfacial pressure, and f the coefficient of friction. Because of symmetry, this frictional heating problem is equivalent to a semi-infinite region $y \geqslant 0$ that is initially at the ambient temperature, θ_a, throughout $y \geqslant 0$, and which at time $t = 0$ is subjected to a uniform heat rate $q_0/2$ at $y = 0$. For this problem, the temperature distribution at the interface $y = 0$, $\theta(0, t)$, at time t is known to be [5]

$$\Theta(0, t) = \Theta_0 = \frac{q_0}{k}\left[\frac{\alpha t}{\pi}\right]^{1/2} = \frac{fp_0w_0}{k}\left[\frac{\alpha t}{\pi}\right]^{1/2} \tag{2}$$

where $\Theta = \theta(y, t) - \theta_a$ is the local temperature in excess of the ambient, k is the thermal conductivity of the material, $\alpha = k/\varrho c$ is the thermal diffusivity, ϱ its density, and c the specific heat of the material.

The time, t_m, for the interface to attain the transition/melting temperature, Θ_m, is then given by

$$t_m = \frac{\pi}{\alpha}\left[\frac{k\Theta_m}{fp_0w_0}\right]^2 \tag{3}$$

During this interval, the effect of the heat flux will have "penetrated" a distance

$$y_m = (4\alpha t_m)^{1/2} = (4\pi)^{1/2}\frac{k\Theta_m}{fp_0w_0} \tag{4}$$

This analysis has two shortcomings. First, the properties of the material have been assumed to be temperature independent. Many of the properties of polymers, such as the specific heat, are known to be quite sensitive to the temperature. Second, a constant heat rate is assumed at the rubbing interface. While this assumption is reasonable for the case in which the rubbing velocity attains the steady-state value in much less time than the time for melt initiation, it needs to be modified for the case in which the rubbing velocity, or the weld pressure, changes with time. There is evidence (Fig. 3 in [1]) that the weld pressure builds up to the steady-state value linearly with time. In that case frictional heating would be more appropriately modelled by allowing the heat rate, q_0, to increase linearly with time. The resulting temperature history could then be easily computed [5].

Because of lack of spin-welding data for Regime I (Fig. 2), this phase will not be analysed in any further detail. The results of this section have been used in Section 6.4 to estimate the times required to initiate melting in PMMA, PVC, acetal and nylon 66, by using Crawford and Tam's data [1].

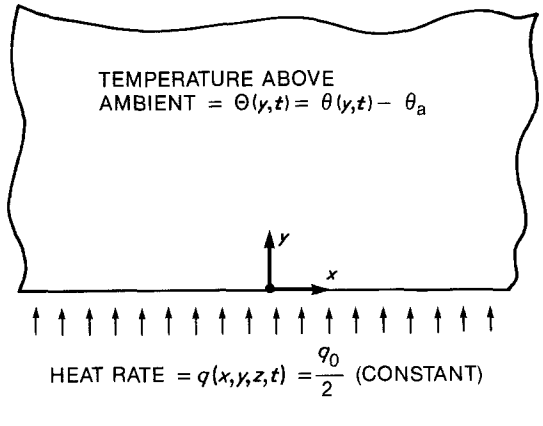

Figure 4 Geometry of the model problem for frictional heating.

4. Steady-state melting and flow (Regime III)

This section addresses the analysis of the steady-state melting and flow regime. It includes an analysis of the heat-affected zone in the solid material.

4.1. Lateral (radial) flow

The actual geometry for the spin welding of tubes is shown in Fig. 1, in which one tube (here the top tube) spins relative to the second tube with an angular velocity, ω. As mentioned above, for most applications the radial thickness, b, of the tube will be much larger than the mean tube radius, r_m. In this analysis it will be assumed that $b \gg r_m$. Then, the spin-welding problem may be treated as being equivalent to the one-dimensional problem, shown in Fig. 3, in which a specimen of thickness b slides on another specimen of the same thickness with a constant sliding velocity $w_0 = r_m\omega$. With reference to Fig. 3, the specimens will be assumed to have infinite dimensions in the y- and z-directions.

During the steady-state phase of the spin-welding process (Regime III in Fig. 2), the rate at which the material is melting at the solid–liquid interface equals the rate at which the melt is being extruded out radially at the lateral cylindrical surfaces of the tube. In this first analysis of the problem, the molten polymer will be modelled as a constant-property newtonian fluid.

The model geometry for the problem is shown in Fig. 5. The stationary surface is at $y = 0$. The moving surface is at $y = h_0$, where h_0 is the steady-state thickness of the molten film. Thus, under steady-state conditions, the melting solid–liquid interfaces will always be at $y = 0$ and $y = h_0$. The thickness, b, in the x-direction is assumed to be much larger than h_0. The

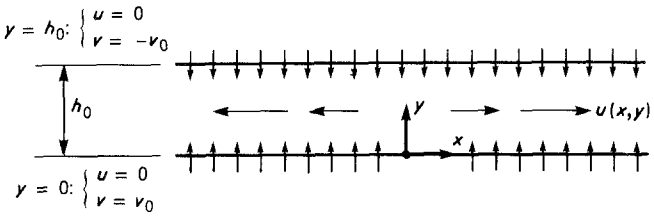

Figure 5 Geometry of the steady-state melting and flow model.

steady-state melting of the polymer at the interfaces $y = 0$ and $y = h_0$ may be modelled by a fluid influx velocity, v_0, that is uniform over the interface. The flow problem then reduces to solving the Navier–Stokes and continuity equations

$$\varrho\left(\frac{\partial \boldsymbol{v}}{\partial t} + \boldsymbol{v}\cdot\nabla\boldsymbol{v}\right) = -\nabla p + \mu\nabla^2\boldsymbol{v} \tag{5}$$

$$\dot{\varrho} + \varrho\nabla\cdot\boldsymbol{v} = 0 \tag{6}$$

for the velocity $\boldsymbol{v} = (u, v, w)$, in the region $-b/2 \leqslant x \leqslant -b/2$, $0 \leqslant y \leqslant h_0$, subject to the boundary conditions

$$\left.\begin{aligned} &u = 0, v = v_0, w = 0 \text{ at } y = 0\\ &u = 0, v = -v_0, w = w_0 \text{ at } y = h_0\\ &p = p_a \text{ at } y = 0 \text{ and } x = \frac{b}{2}\end{aligned}\right\} \tag{7}$$

where p_a is the atmospheric pressure.

Because of symmetry, it may be assumed that $\partial/\partial z \equiv 0$. Furthermore, because $b \gg h_0$, and because of the type of boundary conditions, it may also be assumed that $w = w(y)$.

As indicated in [2], the appropriate Reynolds number, which is the ratio of the inertia to the viscous force, for this problem is

$$R = \frac{\varrho v_0 h_0}{2\mu} \tag{8}$$

For typical spin-welding applications, $R \approx 10^{-6}$ (see discussion in Sections 6.1 and 6.2). The steady-state flow is then a very low Reynolds number flow in which the inertia terms in Equation 5 can be neglected, and the Navier–Stokes equation replaced by

$$\nabla p = \nabla^2\boldsymbol{v} \tag{9}$$

which governs this low Reynolds number "creeping flow."

Subject to the boundary conditions in Equation 7, the solution of Equation 9 for an incompressible fluid comes out to be

$$u = \frac{12v_0}{h_0^3}x(h_0 y - y^2) \tag{10}$$

$$v = v_0\left[1 - \frac{6y^2}{h_0^2} + \frac{4y^3}{h_0^3}\right] \tag{11}$$

$$w = \frac{w_0}{h_0}y \tag{12}$$

$$p - p_a = \frac{12\mu v_0}{h_0^3}\left[\frac{b^2}{4} - x^2 - h_0 y + y^2\right] \tag{13}$$

Let the load per unit length in the z-(circumferential) direction be F. Then

$$\begin{aligned} F &= 2\int_0^{b/2}(p - p_a)|_{y=0}\,dx\\ &= \frac{2\mu v_0}{h_0^3}b^3\end{aligned}$$

so that the average pressure, p_0, applied to the solid surfaces is given by

$$p_0 = \frac{2\mu v_0 b^2}{h_0^3} \tag{14}$$

From Equation 12 the wall shear stress is

$$\begin{aligned} \tau_w &= \tau_{yz}\\ &= \mu\left(\frac{\partial w}{\partial y} + \frac{\partial v}{\partial z}\right)\\ &= \frac{\mu w_0}{h_0}\end{aligned} \tag{15}$$

The torque, T_0, required for spin welding is then

$$\begin{aligned} T_0 &= \int_A r\tau_w\,dA\\ &= r_m\tau_w\int_A dA\\ &= 2\pi r_m^2 b\tau_w\\ &= 2\pi\mu\frac{r_m^2 b w_0}{h_0}\end{aligned}$$

that is,

$$T_0 = 2\pi\mu\frac{r_m^2 b w_0}{h_0} \tag{16}$$

An elimination of μ between Equations 14 and 16 then gives

$$h_0^2 = \frac{bT_0 v_0}{\pi r_m^2 p_0 w_0} \tag{17}$$

From Equations (14) and (16) it also follows that

$$\begin{aligned} \mu &= \frac{h_0 T_0}{2\pi r_m^2 b w_0}\\ &= \frac{1}{2\pi^{3/2} r_m^3}\left[\frac{T_0}{w_0}\right]^{3/2}\left[\frac{v_0}{bp_0}\right]^{1/2}\end{aligned} \tag{18}$$

In the tests described by Crawford and Tam [1], the quantities p_0 and w_0 are controlled while T_0 and v_0 are measured. Equations 17 and 18 then provide means for a direct determination of the film thickness, h_0, and the mean viscosity, μ. In this sense a vibration welding experiment is different from spin welding, because, in the former, the friction force during welding (which would be the "analogue" of the torque in spin welding) is difficult to measure. The additional equation for vibration welding is provided by the energy equation,

which, for spin welding would only provide a check on the viscosity–temperature relationship for the polymer.

In Sections 6.1 and 6.2, Equations 17 and 18 have been used to estimate the film thickness, h_0, and the viscosity, μ, respectively, in PMMA, PVC, acetal and nylon 66 by using Crawford and Tam's data [1].

4.2. Steady-state energy balance

Under steady-state conditions, the work done on the system goes into melting the solid at a steady rate. The geometry for energy balance is shown in Fig. 6. Solid material at the ambient temperature, θ_a, is first heated to the transition/melting temperature, θ_0, at the solid–liquid interface. The molten film undergoes a further increase in temperature to a mean liquid temperature, θ_l. The temperature in the solid can be assumed to depend only on y.

The heat rate per unit length in the z-direction, Q, required for converting the material from a solid at temperature, θ_a, to a liquid at θ_l, is

$$Q = (2b\varrho_l v_0)[\lambda + \bar{c}(\theta_l - \theta_a)] \quad (19)$$

where ϱ_l is the density of the liquid, λ is the latent heat for the (crystalline) material, c is the specific heat of the polymer, and $\bar{c}$ is the mean specific heat over the temperature range (θ_a, θ_l), defined by

$$\bar{c}(\theta_l - \theta_a) = \int_{\theta_a}^{\theta_l} c \, d\theta \quad (20)$$

The rate at which work is being done on the system, per unit length in the z-direction, is $W = W_p + W_s$, where W_p, the work done by the pressure, p_0, in pushing the material at a rate $2v_0$, is

$$W_p = 2p_0 v_0 b \quad (21)$$

and W_s, the rate of work being done by the shear stresses, is given by

$$W_s = b\tau_w w_0 = \frac{\mu b w_0^2}{h_0} \quad (22)$$

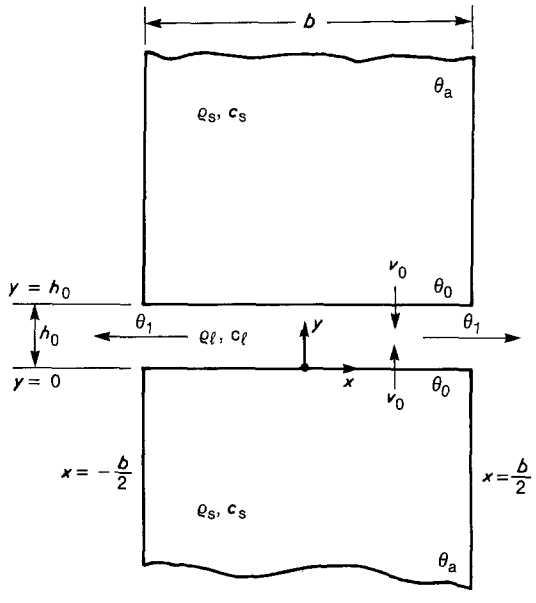

Figure 6 Geometry for steady-state energy balance.

It follows that

$$W = 2p_0 v_0 b + \mu b \frac{w_0^2}{h_0} \quad (23)$$

and, from Equation 16 that

$$\frac{W_p}{W_s} = \frac{2p_0 v_0 h_0}{\mu w_0^2} = \frac{4\pi r_m^2 b p_0 v_0}{T_0 w_0} \quad (24)$$

Equating the rate of working in Equation 23 to the heat rate in Equation 19 results in

$$R = \frac{\varrho v_0 h_0}{2\mu} = \frac{w_0^2}{4\left[\lambda + \bar{c}(\theta_l - \theta_a) - \frac{p_0}{\varrho_l}\right]} \quad (25)$$

For most cases of interest $W_p \ll W_s$, so that the Reynolds number can be well approximated by

$$R = \frac{w_0^2}{4[\lambda + \bar{c}(\theta_l - \theta_a)]} \quad (26)$$

This formula is remarkable in that the steady-state Reynolds number, R, is determined by the weld velocity, the physical properties of the polymer, and the molten-film temperature – which, as a first approximation, may be assumed to equal the glass-transition/melt temperature of the polymer.

As mentioned in Section 4.1, as the quantities p_0, w_0, T_0 and v_0 are known in a spin-welding experiment, Equations 7 and 18 can be used for determining the steady-state film thickness, h_0, and the viscosity, μ. Then, the temperature–viscosity relationship for the polymer can be used to estimate the film temperature. However, the energy balance for the system provides another means for directly determining the mean film exit temperature: From Equations 16 and 25

$$\lambda + \bar{c}(\theta_l - \theta_a) = \frac{p_0}{\varrho_l} + \frac{1}{4\pi\varrho_l b r_m^2}\left[\frac{T_0 w_0}{v_0}\right] \quad (27)$$

As the right-hand side of this equation is fully determinate from test data, a determination of θ_l requires the mean specific heat $\bar{c}$, and the latent heat of fusion λ, which is zero for amorphous polymers.

By using the data of Crawford and Tam [1], Equation 25 has been used in Sections 6.1 and 6.2 to estimate the mean exit film temperature in PMMA, PVC and nylon 66.

4.3. Steady-state temperature profile in the weld specimen

For the steady-state heat transfer into the solid weld specimen, the geometry is the same as in Fig. 6, except that the solid–liquid interface is at the plane $y = 0$. With respect to this coordinate system, the solid material is moving at a constant velocity $v = -v_0$ in the negative y-direction. The appropriate steady-state conduction equation for the temperature, θ, for this one-dimensional problem is

$$\frac{d^2\theta}{dy^2} + \frac{\varrho c v_0}{k}\frac{d\theta}{dy} = 0 \quad (28)$$

which, subject to the boundary conditions $\theta = \theta_0$ at $y = 0$, and $\theta = \theta_a$ as $y \to \infty$, has the solution

$$\frac{\theta - \theta_a}{\theta_0 - \theta_a} = \exp(-\beta y), \quad \beta = \frac{v_0}{\alpha} \tag{29}$$

where $\alpha = k/\varrho c$ is the thermal diffusivity of the solid polymer.

Under steady-state conditions, the heat flux into the solid specimen at the interface $y = 0$ is given by

$$q_0 = \varrho c v_0(\theta_0 - \theta_a) \tag{30}$$

Let y_0 be the depth at which $(\theta - \theta_a)$ is within 1% of $\theta_0 - \theta_a$, i.e. at which $(\theta - \theta_a)/(\theta_0 - \theta_a) = 0.01$. Then, from Equation 29

$$y_0 = 4.6\frac{\alpha}{v_0} \tag{31}$$

In Section 6.3, this equation has been used to estimate y_0 for PMMA, PVC, acetal and nylon 66.

5. Transient melting and flow (Regime II)

Melting at the interface of the two solid rubbing surfaces initiates at the end of Regime I when the interface temperature reaches the melting temperature.

Let the molten film thickness be $h = h(t)$ at time t. The rate of shear work $W_s = \mu b w_0^2/h$ (see Equation 22) is very high during the initial part of the transient phase when h is small. As a result, the rate, v_t, at which the interface is melting, will be much higher than the steady-state rate, v_0. Furthemore, low values of h result in large viscous forces, because of which the lateral velocity, u, is very small for a given constant pressure, p_0. Both these effects, namely the higher melting rate and the low flow velocities, cause the film thickness to increase with time. However, an increase in the film thickness causes a reduction in the rate of shear work and hence a reduction in the melt velocity, v_t. Also an increased film thickness makes lateral fluid flow easier. Both these effects result in a slowing down of the rate at which the film thickness is increasing. Eventually, equilibrium is reached at a film thickness, h_0, at which the rate at which the material is melting at the interface equals the rate of lateral outflow.

The geometry for the process is the same as in Fig. 5, except that the current film thickness is $h(t)$.

5.1. Energy balance

Because the film thickness, h, is increasing at a rate $\dot{h} = \mathrm{d}h/\mathrm{d}t$, the two parts being welded approach each other at a velocity $(2v_t - \dot{h})$. The rate at which the pressure p_0 does work is then

$$W_p = p_0 b(2v_t - \dot{h}) \tag{32}$$

The rate of work being done by the shear stresses is

$$W_s = \frac{\mu b w_0^2}{h} \tag{33}$$

so that the total rate at which work is being done on the system, $W = W_p + W_s$, is

$$W = p_0 b(2v_t - \dot{h}) + \frac{\mu b w_0^2}{h} \tag{34}$$

A part, Q_s, of this work rate is conducted into the solid at the solid–liquid interface. The remainder goes into melting the solid at a temperature, θ_0, and into raising the temperature of the melt to θ_1. It follows that

$$W = 2b\varrho_1 v_t[\lambda + \bar{c}(\theta_1 - \theta_0)] + Q_s \tag{35}$$

Now the temperature in the solid is essentially the ambient temperature, Q_a, except in a very thin layer (Sections 4.3 and 6.3). Furthermore, because v_t is larger in the transient phase, this "boundary layer" can be expected to be even smaller. As a first approximation it will therefore be assumed that the solid arriving at the melt interface is at the ambient temperature, θ_a. Then, Equation 35 can be written as

$$W = 2b\varrho_1 v_t[\lambda + \bar{c}(\theta_1 - \theta_a)] \tag{36}$$

In most cases $W_p \ll W_s$ in the steady case (Section 4.2). Although $v_t > v_0$ in the transient case, its effect is reduced by $\dot{h}$. At the same time W_s is larger because $h < h_0$. Therefore, even in the transient case W_p will be neglected in comparison to W_s. Then, from Equations 34 and 36

$$hv_t = \frac{\mu w_0^2}{2\varrho_1[\lambda + \bar{c}(\theta_1 - \theta_a)]} \tag{37}$$

which, on comparison with Equation 26, results in

$$hv_t = h_0 v_0 \tag{38}$$

It follows that the transient flow is also a very low Reynolds number flow for which the inertia terms in the equations of motion can be neglected.

5.2. Transient flow

The transient flow is then determined by Equation 9. However, the boundary conditions are different from those for the steady-state case given in Equation 7. Although $u = 0$ at both $y = 0$ and $y = h$, just as in Equation 7, the boundary conditions on v are different. Because the film thickness is increasing at a rate $\dot{h}$, the appropriate conditions on v are

$$\left.\begin{aligned} v &= (v_t - \dot{h}/2) \text{ at } y = 0 \\ v &= -(v_t - \dot{h}/2) \text{ at } y = h \end{aligned}\right\} \tag{39}$$

Subject to these boundary conditions, the transient flow field is described by

$$\left.\begin{aligned} u &= \frac{12}{h^3}\left(v_t - \frac{\dot{h}}{2}\right)x(hy - y^2) \\ v &= \left(v_t - \frac{\dot{h}}{2}\right)\left[1 - \frac{6y^2}{h^2} + \frac{4y^3}{h^3}\right] \end{aligned}\right\} \tag{40}$$

$$p_0 = \frac{2\mu b^2}{h^3}\left(v_t - \frac{\dot{h}}{2}\right) \tag{41}$$

The transient nature of these "quasi-steady" solutions stems from the time-dependence of v_t and h.

By using Equations 38 and 41 to eliminate v_t, and by making use of Equation 14 to simplify the resulting expression, the equation governing the time evolution of the film thickness comes out to be

$$h\frac{\mathrm{d}h}{\mathrm{d}t} = \frac{p_0}{\mu b^2}(h_0^4 - h^4) \tag{42}$$

the solution to which, subject to the initial condition $h = 0$ at $t = 0$, is

$$h = h_0(\tanh \gamma t)^{1/2},$$

$$\gamma = \frac{2p_0h_0^2}{\mu b^2} = \frac{4v_0}{h_0} \quad (43)$$

Because $(\tanh 3)^{1/2}$ is within about 0.25% of unity, the time duration, t_0, of the transient (the time for the film thickness to attain its steady-state value h_0) is given by

$$t_0 = \frac{3}{\gamma} = \frac{3}{4}\frac{h_0}{v_t} \quad (44)$$

Thus, the transient phase (Regime II) of the weld lasts for about h_0/v_0 units of time.

Figures illustrating the variations of h/h_0, v_t/v_0 and η/h_0 with the nondimensional time t/γ are given in [2].

Estimates for t_0, based on the data on PMMA, PVC, acetal and nylon 66 given by Crawford and Tam, are discussed in Section 6.5.

6. Analysis of spin-welding data

This section is devoted to an analysis of the spin-welding data generated by Crawford and Tam [1]. They used a specially instrumented spin-welding machine to obtain data on two amorphous thermoplastics, poly(methyl methacrylate) (PMMA) and poly(vinyl chloride) (PVC), and two semicrystalline thermoplastics, acetal and nylon 66. Their data are presented in the form of plots of the steady-state welding torque and the steady-state penetration rate (which they call burn-off) against the weld velocity (which they call the rubbing velocity), with the weld pressure (which they call the axial pressure) as parameter; and plots of the steady-state welding torque and the penetration rate against the weld pressure, with the weld velocity as parameter. All of the data are in the form of smooth curves. Actual data points are only shown for three curves for PMMA.

In addition to the geometrical variables b and r_m, the calculation of the steady-state film thickness, h_0, and the mean film viscosity, μ, via Equations 17 and 18, respectively, requires the weld velocity, w_0, the weld torque, T_0, and the penetration rate, $\dot{\eta} = 2v_0$. These variables have been scaled from the curves in [1], and, for convenience, are listed in the tables in this paper.

The calculation of the mean exit film temperature through Equation 25 requires the density, ϱ, the mean specific heat, $\bar{c}$, and, for semicrystalline polymers, the latent heat of fusion, λ. Now the mean specific heat, $\bar{c}$, depends on the temperature, θ_1. If the dependence of the specific heat on the temperature is known, then $\bar{c}$ and θ_1 can be determined iteratively. However, because the physical properties of the polymers actually tested are not known, only mean generic values of $\bar{c}$ have been used in the analyses in this paper. The uncertainty in the values of λ for the semicrystalline polymers, acetal and nylon 66, is still larger. In spite of these uncertainties, the analysis does determine the trends that can be expected.

All of the tubular specimens tested by Crawford and Tam [1] had a mean radius of $r_m = 5.05$ mm and a radial tube thickness of $b = 2.65$ mm.

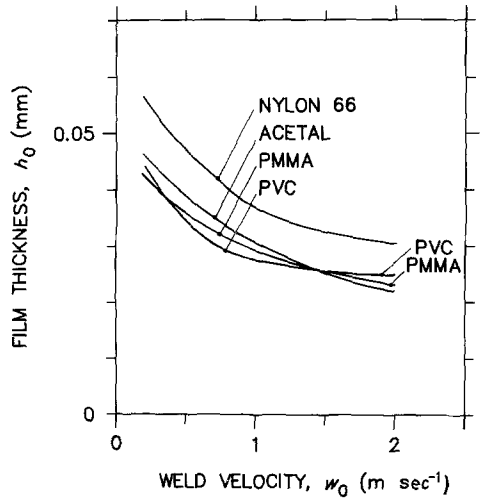

Figure 7 Variation of the film thickness, h_0, with the welding velocity, w_0, at a constant weld pressure of $p_0 = 6.2$ MPa, for four thermoplastics.

6.1. Effect of weld velocity

Steady-state data on the variations of the weld torque, T_0, and the penetration rate, $\dot{\eta} = 2v_0$, with the weld velocity, w_0, at a weld pressure of $p_0 = 6.2$ MPa, for the four thermoplastics PMMA, PVC, acetal and nylon 66 are given, respectively, in Tables I to IV. These data on T_0 and $\dot{\eta}$ have been scaled from the curves in Figs 5 and 9, respectively, in [1]. These data have been used for calculating the film thickness, h_0, and the mean film viscosity, μ, by using Equations 17 and 18, respectively.

For the four polymers, the variations of the film thickness, h_0, with the weld velocity, w_0, at a pressure of $p_0 = 6.2$ MPa are shown in Fig. 7. For each of these four polymers, the film thickness decreases with an increase in the weld velocity. The rate of decrease of h_0 decreases steadily with an increase in w_0.

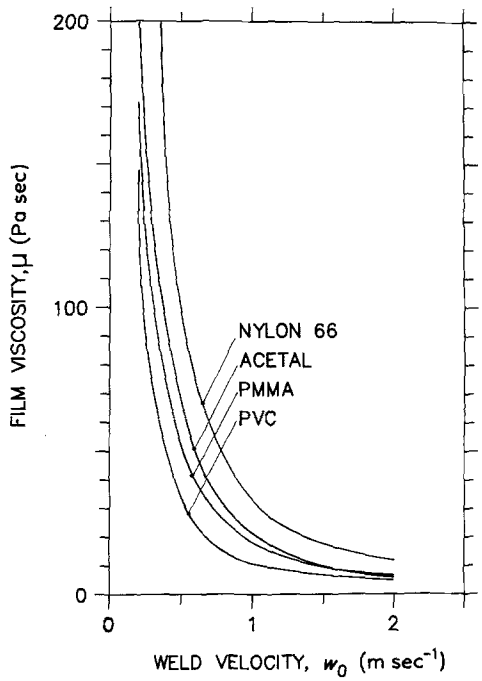

Figure 8 Variation of the film viscosity, μ, with the welding velocity, w_0, at a constant weld pressure of $p_0 = 6.2$ MPa, for four thermoplastics.

TABLE I Spin-welding data and calculated weld parameters for PMMA at a constant weld pressure of 6.2 MPa

w_0 (m sec^{-1})	T_0 (Nm)	$\dot{\eta} = 2v_0$ (mm sec^{-1})	h_0 (mm)	μ (Pa sec)	$\theta_1 - \theta_a$ (°C)	θ_1 (°C)	W_s (kW m^{-1})	$10^2 \frac{W_p}{W_s}$	$10^7 R$	y_0 (mm)	t_0 (10^{-3} sec)
0.2	0.343	0.398	0.043	172.2	236	258	0.42	1.5	0.3	2.63	162
0.4	0.323	0.676	0.038	72.5	261	283	0.81	1.4	1.1	1.55	84
0.6	0.298	0.885	0.034	40.0	276	298	1.12	1.3	2.2	1.2	58
0.8	0.278	1.084	0.032	25.9	280	302	1.37	1.3	4.0	0.97	44
1.0	0.263	1.243	0.030	18.3	288	310	1.62	1.2	6.1	0.84	36
1.2	0.248	1.377	0.028	13.4	294	316	1.83	1.2	8.6	0.76	31
1.4	0.239	1.502	0.026	10.5	303	325	2.10	1.2	11.1	0.70	26
1.6	0.231	1.621	0.025	8.5	311	333	2.31	1.2	14.2	0.65	23
1.8	0.224	1.731	0.024	7.0	317	339	2.50	1.1	17.7	0.61	21
2.0	0.221	1.840	0.023	6.1	327	349	2.81	1.1	20.6	0.57	19

For the same data, the variations of the mean film viscosity, μ, with w_0 are shown in Fig. 8. Apparently, there is a dramatic decrease in viscosity with increasing w_0. By and large, there is a consistent pattern in that the film thickness increases with the mean viscosity.

The data from Figs 5 and 9 in [1], which are listed in Tables I to IV, were used to calculate the mean exit film temperature, θ_1, via Equation 25. The calculated temperatures, θ_1, are based on an ambient room temperature of 22° C. The calculation of θ_1 requires the mean specific heat, $\bar{c}$, and, for semicrystalline polymers, the latent heat of fusion, λ.

The specific heat, and hence the mean specific heat, is temperature dependent. The specific grades of plastics used in the study in [1] were not available. Therefore, the specific heats were assumed to be constant. Furthermore, the values used are more representative of the specific heats near room-temperature conditions, and are therefore lower than the values that would be appropriate for the molten-film temperatures for which the calculations are intended. This was necessitated by the lack of adequate data for the four plastics studied. The effects of these approximations on the calculated temperatures are addressed below.

Reliable latent-heat data for acetal and nylon 66 were not available. As such a "mean" value was used for nylon 66. The film temperature for acetal was not calculated for lack of data on λ. The physical properties used in this paper for calculating film temperatures are listed in Table V [6, 7].

Predicted values of the mean film temperature, θ_1, as a function of the weld velocity, w_0, are shown in Fig. 9. In PMMA the temperature increases with the weld velocity. This is consistent with the decrease in the viscosity (Fig. 8). Furthermore, the curves for both PVC and nylon 66 also exhibit this trend at higher velocities. However, for low weld velocities, the calculated mean film temperatures in PVC and nylon 66 decrease with an increase in the weld velocity. This is inconsistent with the decrease in viscosity under these conditions.

There could be several reasons for this lack of consistency. First, the calculations for the film viscosity and the mean exit film temperature are based on equations that were derived by assuming temperature-independent properties. In actual practice both the viscosity and the film temperature would vary across the film thickness as well as along its length. Second, because constant values have been used for the mean specific heat, $\bar{c}$, the predicted temperatures should be relatively lower at the higher temperatures and relatively higher at the lower temperatures (see Equation 25). The effect of using more realistic temperature-dependent values of $\bar{c}$ would be to decrease the anomalous temperature variation of PVC and nylon 66 at the low end of the weld velocities shown in Fig. 9. Furthermore, an accounting of the increase of $\bar{c}$ with temperature would result in a decrease of the slopes of the curves in Fig. 9. Thus, with an increase in the weld velocity the actual increases in temperature should be smaller than indicated in Fig. 9. Third, there is also the possibility of error in the data. At low weld velocities longer times are required for achieving the steady state. Penetration rates are lower during the transient phase. Therefore there is always the possibility that, at low weld velocities, the reported penetration rates ($2v_0$) are lower than the true steady-state values. It can be seen from Equation 25 that such an error in v_0 would result in a higher estimate for the temperature θ_1.

TABLE II Spin-welding data and calculated weld parameters for PVC at a constant weld pressure of 6.2 MPa

w_0 (m sec^{-1})	T_0 (Nm)	$\dot{\eta} = 2v_0$ (mm sec^{-1})	h_0 (mm)	μ (Pa sec)	$\theta_1 - \theta_a$ (°C)	θ_1 (°C)	W_s (kW m^{-1})	$10^2 \frac{W_p}{W_s}$	$10^7 R$	y_0 (mm)	t_0 (10^{-3} sec)
0.2	0.28	0.53	0.044	147	194	216	0.35	2.5	0.6	2.12	125
0.4	0.225	0.94	0.038	50	177	199	0.56	2.7	2.5	1.19	61
0.6	0.193	1.22	0.032	24	175	197	0.72	2.8	5.7	0.92	39
0.8	0.17	1.5	0.029	15	168	190	0.88	2.9	10.2	0.75	29
1.0	0.17	1.7	0.028	11	184	206	1.04	2.6	15.3	0.66	25
1.2	0.17	1.94	0.027	9.0	194	216	1.27	2.5	20.5	0.58	21
1.4	0.168	2.14	0.026	7.4	202	224	1.48	2.4	26.5	0.52	18
1.6	0.168	2.36	0.026	6.4	209	231	1.67	2.3	33.8	0.48	17
1.8	0.166	2.55	0.025	5.4	215	237	1.85	2.2	41.6	0.44	15
2.0	0.166	2.73	0.025	4.8	223	245	2.04	2.2	50.1	0.41	14

TABLE III Spin-welding data and calculated weld parameters for acetal at a constant weld pressure of 6.2 MPa

w_0 (m sec^{-1})	T_0 (Nm)	$\dot{\eta} = 2v_0$ (mm sec^{-1})	h_0 (mm)	μ (Pa sec)	W_s (kW m^{-1})	$10^2 \frac{W_p}{W_s}$	$10^7 R$	y_0 (mm)	t_m (10^{-3} sec)	t_0 (10^{-3} sec)
0.2	0.4	0.4	0.046	217	0.5	1.3	0.3	2.65	96	173
0.4	0.37	0.7	0.042	90.4	0.91	1.2	1.2	1.51	24	90
0.6	0.345	0.9	0.037	50.3	1.30	1.1	2.4	1.18	11	62
0.8	0.315	1.07	0.034	31.1	1.55	1.1	4.2	0.99	6.0	48
1.0	0.295	1.21	0.031	21.4	1.81	1.1	6.2	0.87	3.8	38
1.2	0.272	1.34	0.028	15.2	2.07	1.1	8.8	0.79	2.7	31
1.4	0.255	1.44	0.026	11.3	2.26	1.1	11.8	0.73	2.0	27
1.6	0.235	1.53	0.025	8.5	2.31	1.1	16.0	0.69	1.5	25
1.8	0.2225	1.6	0.023	6.7	2.50	1.1	19.5	0.66	1.2	22
2.0	0.2125	1.736	0.022	5.5	2.65	1.1	24.7	0.61	1.0	19

TABLE IV Spin-welding data and calculated weld parameters for nylon 66 at a constant weld pressure of 6.2 MPa

w_0 (m sec^{-1})	T_0 (Nm)	$\dot{\eta} = 2v_0$ (mm sec^{-1})	h_0 (mm)	μ (Pa sec)	$\theta_1 - \theta_a$ (°C)	θ_1 (°C)	W_s (kW m^{-1})	$10^2 \frac{W_p}{W_s}$	$10^7 R$	y_0 (mm)	t_m (10^{-3} sec)	t_0 (10^{-3} sec)
0.2	0.6	0.4	0.057	399	290	312	0.74	0.88	0.3	2.88	96	214
0.4	0.51	0.74	0.050	150.5	260	282	1.28	0.96	0.7	1.55	24	101
0.6	0.45	0.98	0.044	78.1	260	282	1.69	0.96	1.6	1.17	11	67
0.8	0.405	1.21	0.040	48.1	250	272	2.04	0.98	2.9	0.95	6.0	50
1.0	0.375	1.38	0.037	32.8	255	277	2.35	0.97	4.4	0.83	3.9	40
1.2	0.355	1.56	0.035	24.4	257	279	2.66	0.96	6.4	0.74	2.7	34
1.4	0.345	1.69	0.033	19.3	273	295	3.04	0.92	8.2	0.68	2.0	29
1.6	0.335	1.85	0.032	15.8	277	299	3.35	0.88	10.7	0.62	1.5	26
1.8	0.33	1.98	0.031	13.4	290	312	3.71	0.88	13.1	0.58	1.2	23
2.0	0.33	2.12	0.031	11.9	304	326	4.07	0.85	15.7	0.54	1.0	22

Equation 27 shows that the exit temperature, θ_1, in semicrystalline polymers is affected by the latent heat, λ, through a subtractive term $\lambda/\bar{c}$. Thus, an error in λ would shift the $\theta_1 - w_0$ curve for nylon 66, in Fig. 9, upwards or downwards: higher values of λ would result in lower film temperatures. The effects of the uncertainties in the values of λ and the temperature dependence of $\bar{c}$ on the predicted values of θ_1 can be illustrated by the physical-properties data for nylon 66. Pickett [7] gives a range of values for the specific heat of nylon 66: $c = 1.46\,\text{kJ kg}^{-1}\text{K}^{-1}$ at 25° C, $c = 2.0$ at 100° C, and $c = 2.34$ at 180° C. Also $\bar{c} = 2.3\,\text{kJ kg}^{-1}\text{K}^{-1}$ over the temperature range of 20 to 250° C. Pickett [7] also gives the value of λ to be in the range of 75.3 to 200.8 kJ kg^{-1}. In the calculations in this paper the values of c and λ used are $\bar{c} = 1.68\,\text{kJ kg}^{-1}\text{K}^{-1}$ and $\lambda = 138\,\text{kJ kg}^{-1}$, giving $\lambda/\bar{c} = 82°$ C. First consider the effect of using a higher value of the specific heat. For the weld parameters in row 1 in Table IV, a value of $\bar{c} = 2.34\,\text{kJ kg}^{-1}\text{K}^{-1}$ (which is more appropriate for high temperatures than the value $\bar{c} = 1.68$ used in Table IV) and $\lambda = 138\,\text{kJ kg}^{-1}$ would result in $\theta_1 = 230°$ C, instead of the value of $\theta_1 = 312°$ C listed in Table I – a temperature reduction of some 82° C. To consider the effect of the value of λ, choose $\bar{c} = 2.34\,\text{kJ kg}^{-1}\text{K}^{-1}$. Then for $\lambda = 75.3$, 138 and 200.8 kJ kg^{-1} the exit temperatures for the weld process parameters in row 1 of Table IV would be 257, 230 and 203° C, respectively. This analysis points out the need for using accurate values of $\bar{c}$ and λ for determining the mean exit temperature.

Without using more accurate physical properties for the polymers, it is difficult to assess which polymer attains the highest temperature at any given weld

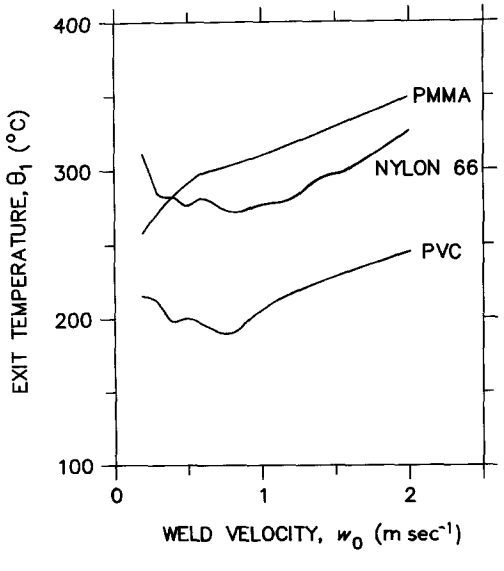

Figure 9 Variation of the mean exit film temperature, θ_1, with weld velocity, w_0, at a constant weld pressure of $p_0 = 6.2$ MPa.

TABLE V Physical properties of polymers studied

Property	PMMA	PVC	Acetal	Nylon 66
Density, ϱ (g cm^{-3})	1.19	1.41	1.42	1.14
Specific heat, c (kJ kg^{-1} K^{-1})	1.47	0.93	1.47	1.68
Latent heat of fusion, λ (kJ kg^{-1})	0	0	–	138
Thermal conductivity, k (W m^{-1} K^{-1})	0.2	0.16	0.24	0.24
Thermal diffusivity, α (mm^2 sec^{-1})	0.114	0.122	0.115	0.125
Coefficient of friction, f	0.41	0.35	0.52	0.76
Melting temperature, θ_m (°C)	–	–	181	265

TABLE VI Spin-welding data and calculated weld parameters for PMMA at a constant weld velocity of 1.21 m sec^{-1}

p_0 (MPa)	T_0 (Nm)	$\dot{\eta} = 2v_0$ (mm sec^{-1})	h_0 (mm)	μ (Pa sec)	$\theta_1 - \theta_a$ (°C)	θ_1 (°C)	W_s (kW m^{-1})	$10^2 \frac{W_p}{W_s}$	$10^7 R$	y_0 (mm)	t_0 (10^{-3} sec)
1	0.066	0.42	0.020	2.5	257	279	0.49	0.22	10.0	2.50	71
1.5	0.103	0.62	0.024	4.8	271	293	0.78	0.32	9.2	1.69	58
2	0.147	0.9	0.030	8.6	267	289	1.11	0.43	9.3	1.17	50
2.5	0.182	1.03	0.032	11.3	289	311	1.37	0.50	8.7	1.02	47
3	0.213	1.11	0.033	13.6	314	336	1.6	0.55	8.0	0.94	45
3.5	0.229	1.17	0.032	14.4	314	336	1.76	0.63	7.7	0.90	41
4	0.234	1.22	0.031	14.2	315	337	1.78	0.73	7.9	0.86	38
5	0.241	1.29	0.029	13.7	307	329	1.83	0.94	8.1	0.81	34
6	0.247	1.38	0.028	13.4	295	317	1.86	1.2	8.6	0.76	30
7	0.254	1.45	0.027	13.3	289	311	1.91	1.4	8.8	0.72	28
8	0.262	1.53	0.026	13.3	284	306	1.98	1.6	8.9	0.69	25
9	0.267	1.62	0.026	13.3	274	296	1.98	1.9	9.4	0.65	24
10	0.278	1.7	0.025	13.8	272	294	2.14	2.1	9.2	0.62	22
11	0.281	1.77	0.025	13.6	265	287	2.11	2.4	9.7	0.59	21
12	0.288	1.85	0.025	13.8	260	282	2.14	2.7	10.0	0.57	20

condition. However, it would seem that PMMA and nylon 66 attain higher temperatures than does PVC. This is in agreement with the experimental observations of Crawford and Tam [1].

The shear power input into the system per unit length in the (circumferential) z-direction, W_s, is listed in Tables I to IV (see Equation 22). Also listed is the ratio of the rate at which the pressure, p_0, is doing work, W_p, to W_s. It is evidence that W_p/W_s is of the order 10^{-2} or smaller. Thus, the shear power rate W_s, which increases with the weld velocity, w_0, is a good measure of the total power input into the system.

The values of the Reynolds number, $R = \varrho v_0 h_0/2\mu$, listed in these tables show that R is of the order 10^{-6} or smaller.

6.2. Effect of weld pressure

Steady-state data for the variations of the weld torque, T_0, and the weld penetration, $\eta = 2v_0$, with the weld pressure, p_0, at a constant weld velocity of $w_0 = 1.21$ m sec^{-1}, for the four plastics, PMMA, PVC, acetal and nylon 66, are given, respectively in Tables VI to IX. These data on the variations of T_0 and $\dot{\eta}$ have been scaled from Figs 7 and 11, respectively, in [1]. As in the previous section, these data have been used for calculating the film thickness, h_0, the mean film viscosity, μ, and the mean exit temperature, θ_1, through Equations 17, 18 and 25, respectively.

The variations of the film thickness with the weld pressure, at a constant weld velocity of $w_0 = 1.21$ m sec^{-1}, are shown in Fig. 10. For each of the four polymers, the film thickness first increases with the weld pressure but then decreases with further increases in p_0. A comparison of Figs 7 and 10 shows that the film thicknesses for any one plastic are of the same order. However, over the ranges of the parameters studied, the weld velocity appears to have a larger effect on h_0 than does p_0.

The corresponding variations of the film viscosity, μ, are shown in Fig. 11. Here again, the viscosity first increases with p_0 and, after attaining a maximum, begins to decrease. However, for $p_0 > 3$ MPa, the viscosities do not vary significantly with an increase in p_0. This is especially true of acetal and PMMA. A comparison of Figs 8 and 11 shows how differently the weld velocity, w_0, and the weld pressure affect the film viscosity, μ. While increases in w_0 result in a dramatic decrease in μ, p_0 has a more moderate effect. The reason for this difference is that increases in p_0 have a small effect on the shear work rate, W_s (see tabulated values of W_s and W_p/W_s in Tables VI to IX), in comparison to the large increases caused by increases in w_0

TABLE VII Spin-welding data and calculated weld parameters for PVC at a constant weld velocity of 1.21 m sec^{-1}

p_0 (MPa)	T_0 (Nm)	$\dot{\eta} = 2v_0$ (mm sec^{-1})	h_0 (mm)	μ (Pa sec)	$\theta_1 - \theta_a$ (°C)	θ_1 (°C)	W_s (kW m^{-1})	$10^2 \frac{W_p}{W_s}$	$10^7 R$	y_0 (mm)	t_0 (10^{-3} sec)
1	0.082	0.98	0.033	5.3	183	205	0.62	0.42	21.5	1.15	51
1.5	0.124	1.46	0.041	9.8	186	208	0.93	0.62	21.5	0.77	42
2	0.141	1.64	0.040	10.9	188	210	1.06	0.82	21.2	0.68	37
2.5	0.151	1.72	0.038	11.1	193	215	1.13	1.0	20.8	0.65	33
3	0.157	1.78	0.036	10.9	194	216	1.17	1.2	20.7	0.63	30
3.5	0.163	1.82	0.034	10.8	197	219	1.23	1.4	20.2	0.62	28
4	0.166	1.86	0.033	10.5	197	219	1.23	1.6	20.6	0.60	27
5	0.171	1.91	0.030	9.9	198	220	1.28	2.0	20.4	0.59	24
6	0.172	1.95	0.028	9.3	196	218	1.29	2.4	20.7	0.58	22
7	0.174	1.99	0.026	8.8	195	217	1.31	2.8	20.7	0.56	20
8	0.176	2.03	0.025	8.5	195	217	1.32	3.2	21.0	0.55	18
9	0.178	2.07	0.024	8.2	194	216	1.33	3.7	21.4	0.54	17
10	0.179	2.1	0.023	7.9	193	215	1.33	4.1	21.5	0.53	16
11	0.181	2.14	0.022	7.7	192	214	1.36	4.6	21.5	0.52	15
12	0.183	2.18	0.021	7.6	192	214	1.40	5.0	21.2	0.51	14

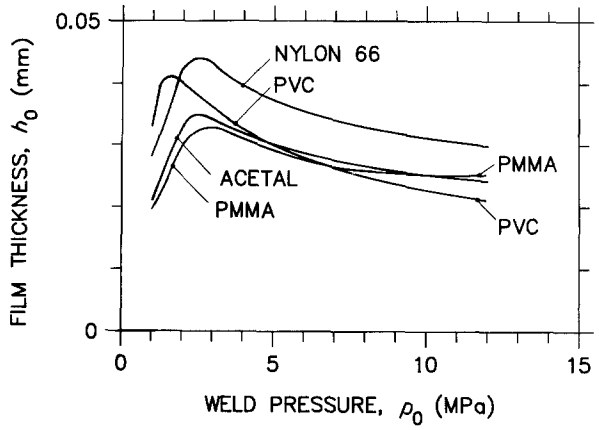

Figure 10 Variation of the film thickness, h_0, with the weld pressure, p_0, at a constant weld velocity of $w_0 = 1.21\,\mathrm{m\,sec^{-1}}$.

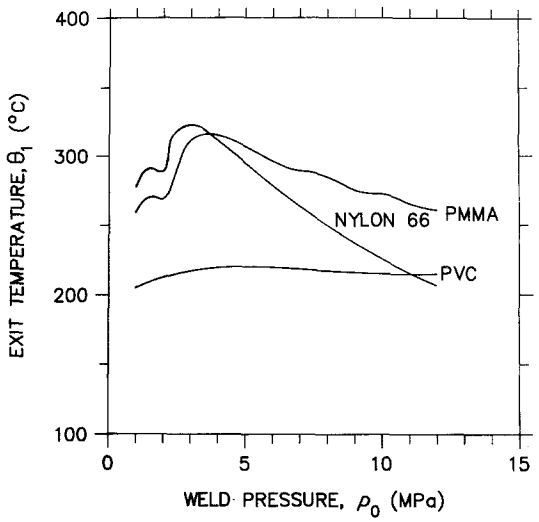

Figure 12 Variation of the mean exit film temperature, θ_1, with the weld pressure, p_0, at a constant weld velocity of $w_0 = 1.21\,\mathrm{m\,sec^{-1}}$.

(Tables I to IV). The smaller changes in energy input cause smaller changes in the viscosity. Here again, W_p/W_s is of the order 10^{-2} or less.

The smaller changes in energy input are also reflected in the relatively smaller changes in the mean exit temperatures, which are shown in Fig. 12. When compared with Fig. 9, the temperature variations are less pronounced in Fig. 12. The temperature variations in Fig. 12 exhibit an anomalous behaviour in that the mean film temperature decreases beyond $p_0 > 4$ MPa while the viscosity decreases. This is especially true of nylon 66. As discussed in Section 6.1, at least some of this anomalous behaviour would be reduced when the temperature dependence of the specific heat is taken into account.

Tables VI to IX also show that the Reynolds number for the process conditions is of the order 10^{-6}.

Steady-state data for the variations of the weld parameters for PMMA with the weld pressure, p_0, for a constant weld velocity of $w_0 = 2\,\mathrm{m\,sec^{-1}}$ are listed in Table X. The data on T_0 and $\dot{\eta}$ have been scaled from Figs 6 and 10, respectively, in [1]. The variations of the film thickness, h_0, the film viscosity, μ, and the mean exit temperature, θ_1, with the weld pressure, p_0, are shown in Figs 13 to 15, respectively, for $w_0 = 1.21\,\mathrm{m\,sec^{-1}}$ and $w_0 = 2\,\mathrm{m\,sec^{-1}}$. As expected, higher velocities contribute to lower film thicknesses and lower viscosities. The mean exit temperature, θ_1, is larger for $w_0 = 2\,\mathrm{m\,sec^{-1}}$ than for $w_0 = 1.21\,\mathrm{m\,sec^{-1}}$ over a range of values of p_0, but not for all values of p_0. This is not consistent with the fact (see Fig. 13) that the viscosity is lower at $w_0 = 2\,\mathrm{m\,sec^{-1}}$ than at $w_0 = 1.21\,\mathrm{m\,sec^{-1}}$ for all values of p_0. The possible reasons for this discrepancy have already been discussed above and in Section 6.1.

6.3. Steady-state temperature profile in weld specimens

The distance y_0 into the solid from the solid–liquid interface, at which the temperature rise, $(\theta - \theta_a)$, is within 1% of $(\theta_0 - \theta_a)$ is given in Equation 31 by $y_0 = 4.6\alpha/v_0$. Values of the thermal diffusivities, α, for the four polymers, as given in Table V, have been used for calculating y_0 under different process conditions. These calculated values of y_0 are listed in Tables I to IV and VI to X. The values of y_0 lie in the range 0.5 to 3 mm. Higher weld velocities and higher weld pressures result in higher values of v_0, and therefore in lower values of y_0. Thus, under steady-state conditions, the temperature rise in the solid material is very localized.

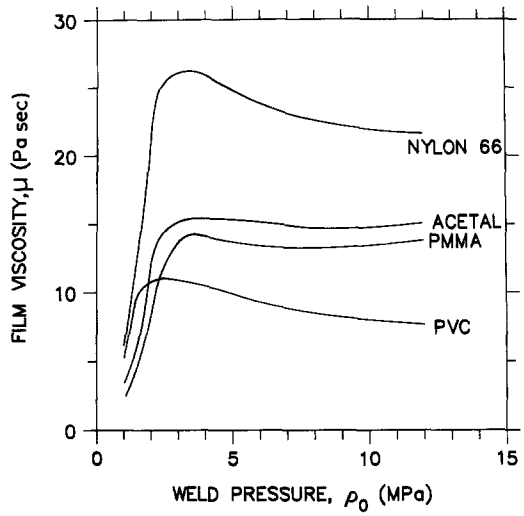

Figure 11 Variation of the film viscosity, μ, with the weld pressure, p_0, at a constant weld velocity of $w_0 = 1.21\,\mathrm{m\,sec^{-1}}$.

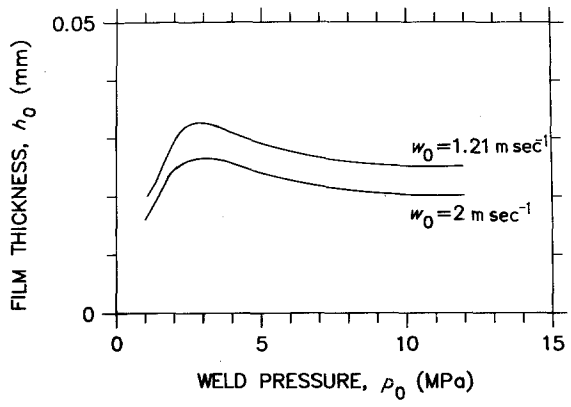

Figure 13 The effect of the weld velocity on the film thickness with weld pressure variation in PMMA.

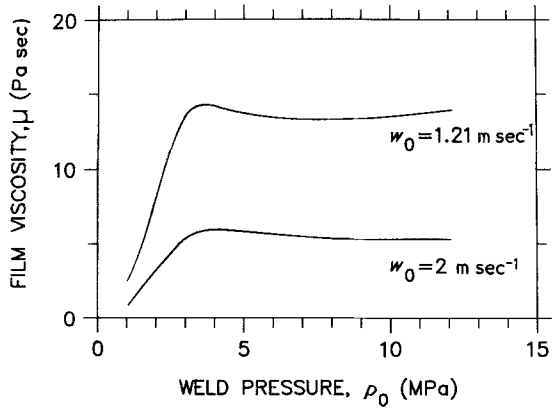

Figure 14 The effect of the weld velocity on the film viscosity with weld pressure variation in PMMA.

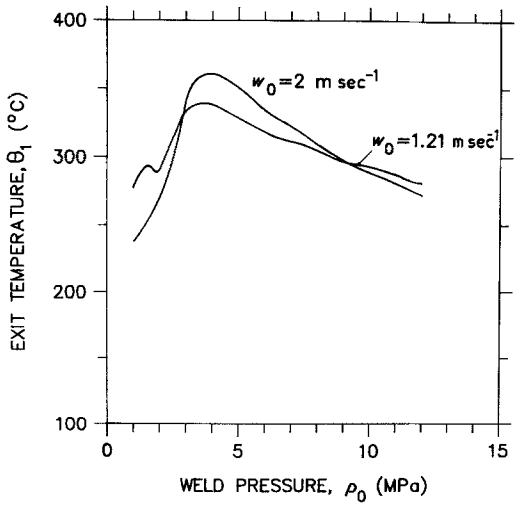

Figure 15 The effect of the weld velocity on the mean exit film temperature with weld pressure variation in PMMA.

6.4. Time required for melt initiation

The time, t_m, required to initiate melting at the rubbing interfaces can be estimated from Equation 3. In addition to other variables, the calculation of t_m requires the coefficient of friction, μ, and the melting temperature, θ_m. For purposes of estimating, t_m, the coefficients of friction are assumed to have the constant values given in Table V [1]. The amorphous polymers do not have a well-defined melting temperature. As such, melt initiation times for PMMA and PVC have not been estimated. The melting points of acetal and nylon 66 are listed in Table V.

The values of t_m, in milliseconds, for acetal and nylon 66 are listed in Tables III and IV, respectively, for a constant weld pressure of 6.2 MPa. As the weld velocity increases from 0.2 to 2 m sec^{-1}, t_m decreases from 96 to 1 m sec for both acetal and nylon 66.

The values of t_m for acetal and nylon 66, for a constant weld velocity of $w_0 = 1.21$ m sec^{-1}, are listed, respectively, in Tables VII and VIII. As p_0 increases from 1 to 12 MPa, t_m decreases from 100 to 0.7 m sec.

6.5. Duration of transient flow

The time duration, t_0, of the unsteady transient flow (Regime II) was estimated in Equation 44 to be $t_0 = 3h_0/4v_0$. Values of t_0 calculated from this equation, for different weld conditions, are listed in the last columns of Tables I to IV and VI to X.

For each of the four polymers, t_0 decreases with increases in both the weld velocity, w_0, and the weld pressure, p_0.

For the process parameters considered, t_0 varies in the range of 12 to 162 m sec for PMMA, 14 to 125 m sec for PVC, 19 to 173 m sec for acetal, and 21 to 214 m sec for nylon 66.

The last two columns in Table III show that, at a constant pressure of $p_0 = 6.2$ MPa, the time for transient flow, t_0, is larger than the time, t_m, for initiation of melting. Their ratio increases at higher velocities. Table VIII shows that, at a constant weld velocity of 1.21 m sec^{-1}, the ratio of t_0 to t_m increases with an increase in the weld pressure. Tables IV and IX show that nylon 66 exhibits similar trends.

Tables VI and X show that, for identical weld pressures, t_0 for PMMA decreases with an increase in the weld velocity.

7. Conclusion

Analytical models have been developed for the first three phases of the spin-welding process. In the first phase (Regime I), friction at the rubbing interface causes the temperature of the interfacial material to rise to the melting temperature. The second phase

TABLE VIII Spin-welding data and calculated weld parameters for acetal at a constant weld velocity of 1.21 m sec^{-1}

p_0 (MPa)	T_0 (Nm)	$\dot{\eta} = 2v_0$ (mm sec^{-1})	h_0 (mm)	μ (Pa sec)	W_s (kW m^{-1})	$10^2 \frac{W_p}{W_s}$	$10^7 R$	y_0 (mm)	t_m (10^{-3} sec)	t_0 (10^{-3} sec)
1	0.0821	0.4	0.021	3.4	0.63	0.17	8.8	2.65	100	79
1.5	0.129	0.62	0.027	6.8	0.98	0.25	8.7	1.71	45	65
2	0.1828	0.88	0.033	11.8	1.39	0.34	8.7	1.20	25	56
2.5	0.213	1.06	0.035	14.6	1.62	0.44	9.0	1.00	16	50
3	0.2278	1.14	0.034	15.2	1.73	0.53	9.1	0.93	11	45
3.5	0.237	1.2	0.033	15.4	1.81	0.62	9.1	0.88	8.2	41
4	0.2464	1.24	0.032	15.5	1.88	0.71	9.1	0.85	6.3	39
5	0.2596	1.29	0.030	15.3	1.98	0.87	9.0	0.82	4.0	35
6	0.2702	1.34	0.029	15.1	2.02	1.0	9.1	0.79	2.8	32
7	0.2781	1.38	0.027	14.8	2.13	1.2	8.9	0.77	2.1	29
8	0.2887	1.42	0.027	14.9	2.14	1.4	9.1	0.75	1.6	29
9	0.2946	1.46	0.026	14.6	2.18	1.6	9.2	0.72	1.2	27
10	0.3046	1.504	0.025	14.8	2.30	1.7	9.0	0.70	1.0	25
11	0.3115	1.548	0.025	14.8	2.30	1.9	9.3	0.68	0.8	24
12	0.3205	1.6	0.024	15.1	2.44	2.1	9.0	0.66	0.7	23

TABLE IX Spin-welding data and calculated weld parameters for nylon 66 at a constant weld velocity of 1.21 m sec^{-1}

p_0 (MPa)	T_0 (Nm)	$\dot{\eta} = 2v_0$ (mm sec^{-1})	h_0 (mm)	μ (Pa sec)	$\theta_1 - \theta_a$ (°C)	θ_1 (°C)	W_s (kW m^{-1})	$10^2 \frac{W_p}{W_s}$	$10^7 R$	y_0 (mm)	t_m (10^{-3} sec)	t_0 (10^{-3} sec)
1	0.113	0.5	0.028	6.1	255	277	0.85	0.16	6.5	2.3	101	84
1.5	0.179	0.76	0.035	12.3	269	291	1.36	0.22	6.2	1.51	45	69
2	0.245	1.05	0.042	20.0	266	288	1.85	0.3	6.3	1.10	25	60
2.5	0.3	1.18	0.044	25.7	298	320	2.27	0.35	5.8	0.97	16	56
3	0.317	1.25	0.043	26.2	297	319	2.36	0.42	5.8	0.92	11	52
3.5	0.329	1.3	0.041	26.2	296	318	2.48	0.49	5.8	0.88	8.3	47
4	0.337	1.36	0.040	26.0	289	311	2.52	0.57	6.0	0.85	6.3	44
5	0.345	1.46	0.037	24.9	272	294	2.61	0.74	6.2	0.79	4.0	38
6	0.35	1.55	0.035	23.9	257	279	2.65	0.93	6.5	0.74	2.8	34
7	0.353	1.64	0.034	23.1	242	264	2.64	1.1	6.9	0.70	2.1	31
8	0.357	1.74	0.033	22.6	227	249	2.66	1.4	7.2	0.66	1.6	28
9	0.361	1.84	0.032	22.3	215	237	2.70	1.6	7.5	0.63	1.2	26
10	0.363	1.93	0.031	21.9	203	225	2.74	1.9	7.8	0.60	1.0	24
11	0.367	2.03	0.030	21.7	193	215	2.81	2.1	8.0	0.57	0.8	22
12	0.371	2.12	0.030	21.6	185	207	2.79	2.4	8.4	0.54	0.7	21

(Regime II) starts with the initiation of melting at the weld interface. During this transient phase the molten film thickness increases from zero to a steady-state value, h_0. The third phase (Regime III) is characterized by a steady state in which the rate of melting of the polymer equals the rate of lateral outflow of the melt. During this phase the film thickness has a constant value, h_0. The film viscosity and temperature are also time independent.

In the analyses presented in this paper, the physical properties of the solid and liquid polymers have been assumed to be constant. While the physical properties of polymers are known to have a strong temperature dependence, the constant-property approximation is adequate for this first analysis of the spin-welding process.

Regime III, the steady-state phase, has been modelled as a low-Reynolds-number flow in which inertia forces can be neglected. This assumption has been validated by Crawford and Tam's [1] data from which the Reynolds number is estimated to be of the order of 10^{-6}.

The analysis of the unsteady (Regime II) phase is more approximate for two reasons. First, additional assumptions have been made in deriving Equation 38. Second, during this phase, the temperature, and hence the viscosity and other physical properties, would vary significantly. These variations are not considered in the analysis. However, with the current inadequate understanding of the spin-welding process, the constant-property transient analysis does provide an insight into the process conditions during the transient phase.

The analytical models have been used for analysing Crawford and Tam's [1] data on the spin welding of PMMA, PVC, acetal and nylon 66. The results show that, at a constant weld pressure, an increase in the weld velocity results in a dramatic decrease in the steady-state viscosity. On the other hand, at a constant weld velocity, the viscosity is not very sensitive to changes in the weld pressure. This difference of viscosity dependence on the weld parameters can be explained in terms of the magnitude of W_p relative to W_s. However, this difference could not have been anticipated without the benefit of the analysis. In general, changes in the weld velocity appear to affect the steady-state film thickness more than do damages in the weld pressure.

The data of Crawford and Tam [1] provide means for evaluating the film thickness, h_0, and the viscosity, μ, without the use of the energy equation. The energy equation then provides an independent means for estimating the exit film temperature. The known temperature dependence of the viscosity can then, in principle, be used as a check for the analytical model. This was not done for the present data [1] because the physical properties of the actual polymers used are not accurately known. In fact, the mean exit film temperatures were estimated by using average generic physical properties.

TABLE X Spin-welding data and calculated weld parameters for PMMA at a constant weld velocity of 2 m sec^{-1}

p_0 (MPa)	T_0 (Nm)	$\dot{\eta} = 2v_0$ (mm sec^{-1})	h_0 (mm)	μ (Pa sec)	$\theta_1 - \theta_a$ (°C)	θ_1 (°C)	W_s (kW m^{-1})	$10^2 \frac{W_p}{W_s}$	$10^7 R$	y_0 (mm)	t_0 (10^{-3} sec)
1	0.051	0.64	0.016	0.99	215	237	0.66	0.27	30.8	1.64	38
2	0.117	1.28	0.025	3.4	247	269	1.44	0.46	28.0	0.82	29
3	0.171	1.47	0.026	5.3	315	337	2.16	0.55	21.5	0.71	27
4	0.20	1.6	0.026	6.1	339	361	2.49	0.68	20.3	0.66	24
5	0.205	1.7	0.024	5.8	328	350	2.56	0.88	20.9	0.62	21
6	0.208	1.82	0.023	5.6	311	333	2.58	1.1	22.2	0.58	19
7	0.212	1.92	0.022	5.5	301	323	2.65	1.3	22.8	0.55	17
8	0.216	2.06	0.021	5.5	287	309	2.78	1.6	23.4	0.51	15
9	0.217	2.16	0.021	5.3	276	298	2.68	1.9	25.5	0.49	15
10	0.221	2.28	0.020	5.3	267	289	2.81	2.2	25.6	0.46	13
11	0.224	2.39	0.020	5.3	259	281	2.81	2.5	26.8	0.44	13
12	0.228	2.52	0.020	5.3	250	272	2.81	2.8	28.3	0.42	12

In one sense, the function of the first three phases (Regimes I to III) of the spin welding process is to generate a molten film, which then solidifies into a weld in the final phase. The thickness, h_0, and the temperature, θ_1, of the steady-state film, which can be estimated by the procedures described in this paper, are important. They determine the cooling rate in the film during the final phase (Regime IV) when the molten film solidifies while still flowing laterally outwards. A control of the cooling rate would be especially helpful for controlling the crystalline morphology in the welds of crystalline polymers.

The mechanisms of heat generation, melting, and flow in spin welding are similar to those in vibration welding. Therefore, for the same polymer, the process conditions in vibration welding can be inferred from equivalent processing conditions in spin welding. This could be useful because of the ease with which torque measurements can be made in spin welding. Equivalent information for vibration welding would require the measurement of the friction force.

Acknowledgement

Special thanks are due to Julia A. Kinloch for her help and patience during the preparation of this paper.

References

1. R. J. CRAWFORD and Y. TAM, *J. Mater. Sci.* **16** (1981) 3275.
2. V. K. STOKES, "Vibration Welding of Thermoplastics – Part I: Phenomenology and Analysis of the Welding Process", Report no. 86CRD223, General Electric Company, Corporate Research and Development, Schenectady, New York (1986).
3. *Idem, Polym. Engng Sci.* **28** (1988) 718.
4. *Idem, ibid.* **28** (1988) 728.
5. H. S. CARSLAW and J. C. JAEGER, "Conduction of Heat in Solids", 2nd Edn (Oxford University Press, London, 1966) p. 75.
6. "Plastics 1980: A Desk-Top Data Bank, Book B", 4th Edn (The International Plastics Selector, 1979).
7. O. A. PICKETT, Jr, in "Polymer Handbook", edited by J. Brandrup and E. H. Immergut (Interscience, New York, 1966) pp. VI-80, 81.

Received 4 August
and accepted 1 December 1987